TECHNISCHE MECHANIK
an open access journal

journal homepage: www.ovgu.de/techmech

Tech. Mech., Vol. 43, Is. 2, (2023), 259–270

Received: 13.06.2023
Accepted: 16.11.2023
Available online: 16.11.2023

Closed-form series solutions to peridynamic rod equations: Influence of kernel function

Zhenghao Yang[1], Konstantin Naumenko[2]*, Chien-Ching Ma[1], and Yang Chen[3]

[1] Department of Mechanical Engineering, National Taiwan University, 10617, Taipei, Taiwan
[2] Otto-von-Guericke-University Magdeburg, Institute of Mechanics, 39106 Magdeburg, Germany
[3] Department of Environmental Engineering Planning and Design, Heilongjiang Academy of Forestry Design and Research, Harbin, China

Abstract: Peridynamics is a generalized continuum theory that takes into account long range internal force/moment interactions. The aim of this paper is to derive closed form analytical solutions for peridynamic rod equations with fixed-fixed and fixed-free boundary conditions. A family of kernel functions is introduced to analyze the influence on the results for rods under distributed static load and free vibrations for different initial conditions. To validate the derived solutions, nonlocal results are compared against classical results for different boundary conditions and horizon sizes. One can observe that when the horizon size approaches zero, the results according the non-local and local theories converge to each other. Introduced kernels indeed play different roles in both statics and dynamics. In particular, the Gauss type kernel function gives the results which are closest to the classical solutions.

Keywords: peridynamics, rod, kernel function, closed-form solution

1 Introduction

In the past decades non-local theories have become increasingly important due to many applications in micro- and nanometer scale components, composite materials with high contrast in properties and laminates with extremely thin layers. To extend the classical continuum mechanics (CCM) higher order deformation gradients can be introduced as arguments of the strain energy density, e.g., Cordero et al. (2016). With a variational principle, a family of strain gradient theories according to a maximal order of the considered deformation gradient can be formulated. For elastic materials, Nth-order gradient terms lead to a system of linear or nonlinear partial differential equations of the 2Nth order Eremeyev (2023). Strain gradient theories lead to higher order stress tensors and as a result require many additional boundary conditions.

Another class of extended continuum theories can be formulated within the framework of peridynamics (PD) Silling and Lehoucq (2010); Silling (2016). Here the balance equations for long-range internal forces are introduced. The deformation gradient, its higher gradients or gradients of internal state variables are not required. Deformation of bond vectors with initially finite length are analyzed in contrast to differential line elements in contrast to classical or gradient extended CCM. Besides several PD theories for three-dimensional solids Silling and Lehoucq (2010), PD formulations for rods Silling et al. (2003), beams Yang et al. (2022b), plates Naumenko and Eremeyev (2022) and shells Chowdhury et al. (2016) are available. The resulting PD equations of motion are of integro-differential type, opposed to strain gradient theories, where partial differential equations are introduced. Numerical methods such as the mesh-free method Silling and Askari (2005) and discontinuous finite element formulation Ren et al. (2017) were developed to solve PD equations of motion numerically. Various examples of numerical are presented in the literature, illustrating the ability of PD to capture complex phenomena such as crack initiation Naumenko et al. (2022), crack branching Mehrmashhadi et al. (2020), and crack kinking Diana and Ballarini (2020), among others.

Despite many numerical results discussed in the literature, analytical solutions to PD integral equations are available only for few simplified problems. For straight axially-loaded rods, closed-form solutions are derived in Mikata (2012); Nishawala and Ostoja-Starzewski (2017); Silling et al. (2003); Weckner and Abeyaratne (2005); Yang et al. (2022a). For initially straight beams with various boundary constraints, series solutions to PD equations are presented in Yang et al. (2022b). Series solutions for Kirchhoff-type plates under special boundary conditions are given in Yang et al. (2022c). General analytical solutions of peristatics and peridynamics for three-dimensional infinite media for an arbitrary body force density, and arbitrary initial conditions are derived in Mikata (2023). Analytical solutions illustrate the influence of PD settings, such as the horizon size, non-locality of boundary conditions, etc. on the deformation state explicitly. Furthermore closed-form analytical solutions are useful to validate the numerical methods developed to solve PD equations and to study the convergence of numerical results.

The aim of this study is to derive closed-form series solutions to peridynamic equations of axially loaded rods. In addition to solutions presented in Yang et al. (2022a), a family of kernel functions is introduced. The results for rods under distributed static load and free vibrations for different initial conditions will be presented. In particular the influence of kernel functions on the axial displacements and natural frequencies will be analyzed.

* E-mail address: konstantin.naumenko@ovgu.de
doi: 10.24352/UB.OVGU-2023-062

2 Peridynamic equation of motion for a rod

The classical equation of motion for elastic rods can be formulated as follows Weaver Jr. et al. (1991)

$$\ddot{u}(x,t) = c\frac{\partial^2 u}{\partial x^2}(x,t), \quad c = \frac{E}{\rho} \tag{1}$$

where u is the displacement, x is the axial coordinate and t is the time variable, ρ is the density and E is the Young's modulus. In order to obtain the corresponding formulation in the non-local framework, one can apply the following Taylor expansion for the displacement

$$u(x+\xi) - u(x) = \left.\frac{\partial u}{\partial x}\right|_x \xi + \frac{1}{2}\left.\frac{\partial^2 u}{\partial x^2}\right|_x \xi^2 + \frac{1}{3!}\left.\frac{\partial^3 u}{\partial x^3}\right|_x \xi^3 + O\left(\xi^4\right), \tag{2}$$

where $\xi = x' - x$ is the coordinate difference between the material point x and its family member x'. Consider a collection of points of the rod centerline Γ and an open ball centered at point x with radius of the PD horizon size δ defined $\forall x \in \Gamma$ as follows

$$H_x := \{x' \in \Gamma : |x' - x| < \delta\} \tag{3}$$

Multiplying each term by a kernel function $\kappa(\xi)$ and integrating over an open ball yields

$$\int_{-\delta}^{\delta} \kappa(\xi)\left[u(x+\xi) - u(x)\right] d\xi = \int_{-\delta}^{\delta} \kappa(\xi)\left[\left.\frac{\partial u}{\partial x}\right|_x \xi + \frac{1}{2}\left.\frac{\partial^2 u}{\partial x^2}\right|_x \xi^2 + \frac{1}{3!}\left.\frac{\partial^3 u}{\partial x^3}\right|_x \xi^3 + O\left(\xi^4\right)\right] d\xi \tag{4}$$

We assume that the kernel $\kappa(\xi)$ satisfies the following conditions

$$\kappa(-\xi) = \kappa(\xi), \quad \text{and} \quad \lim_{\xi\to 0}\left[\xi^2\kappa(\xi)\right] < \infty \tag{5}$$

With the kernel according to Eq. (5), odd terms in Eq. (4) cancel out. By neglecting the truncation error, Eq. (4) can be reduced to

$$\int_{-\delta}^{\delta} \kappa(\xi)\left[u(x+\xi) - u(x)\right] d\xi = \frac{1}{2}\left.\frac{\partial^2 u}{\partial x^2}\right|_x \int_{-\delta}^{\delta} \kappa(\xi)\xi^2 d\xi \tag{6}$$

which gives

$$\left.\frac{\partial^2 u}{\partial x^2}\right|_x = \lambda(\delta)\int_{-\delta}^{\delta} \kappa(\xi)\left[u(x+\xi) - u(x)\right] d\xi, \quad \lambda(\delta) = 2\left[\int_{-\delta}^{\delta} \kappa(\xi)\xi^2 d\xi\right]^{-1} \tag{7}$$

Substituting Eq. (7) into (1) yields the one-dimensional wave equation in the non-local form as follows

$$\ddot{u}(x,t) = c\lambda(\delta)\int_{-\delta}^{\delta} \kappa(\xi)\left[u(x+\xi) - u(x)\right] d\xi \tag{8}$$

Similarly, the one-dimensional non-local Poisson's equation (peristatic equation for the rod) has the following form

$$e\lambda(\delta)\int_{-\delta}^{\delta} \kappa(\xi)\left[u(x+\xi) - u(x)\right] d\xi + f(x) = 0, \quad e = EA, \tag{9}$$

where A is the cross section area of the rod.

2.1 Non-local boundary conditions

The governing equations (8) and (9) are applicable only for the material points whose PD horizon are completely embedded within the body. However, for material points adjacent to the boundary, it is necessary to introduce fictitious material region for the sake of ensuring the validation of the PD formulation. In what follows the width of the fictitious region is selected to be of the PD horizon size, δ, as shown in Fig. 1. Below we consider the homogeneous Dirichlet (fixed) and Neumann (free) boundary conditions (BCs) within nonlocal framework.

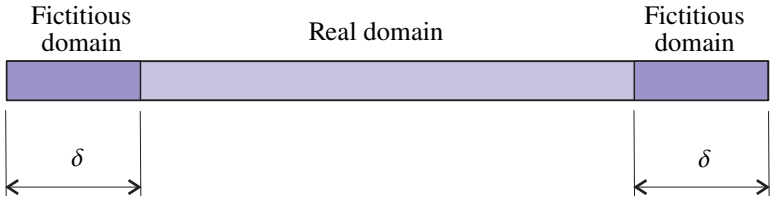

Fig. 1: Real and fictitious domains for the road

2.2 Fixed boundary

In classical theory, cross section fixed at $x = 0$ implies that

$$u(0,t) = 0 \quad \Rightarrow \quad \ddot{u}(0,t) = 0 \quad \Rightarrow \quad \left.\frac{\partial^2 u}{\partial x^2}\right|_{(0,t)} = 0 \tag{10}$$

With the central difference

$$\left.\frac{\partial^2 u}{\partial x^2}\right|_{(0,t)} = 0 \quad \Rightarrow \quad \frac{u(-\xi,t) - 2u(0,t) + u(\xi,t)}{\xi^2} = 0 \tag{11}$$

we obtain

$$u(-\xi,t) = -u(\xi,t) \quad \forall \xi \in [0,\delta] \tag{12}$$

Eq. (12) is called nonlocal homogeneous Dirichlet boundary condition, which admits an anti-symmetric relation about boundary between real and fictitious domain.

2.3 Free boundary

Suppose the following homogenous Neumann boundary condition is applied at $x = L$

$$N = e\left.\frac{\partial u}{\partial x}\right|_{(L,t)} = 0, \tag{13}$$

where N is the normal force. Applying the central difference

$$\left.\frac{\partial u}{\partial x}\right|_{(L,t)} = 0 \quad \Rightarrow \quad \frac{u(L-\xi,t) - u(L+\xi,t)}{2\xi} = 0 \tag{14}$$

it follows

$$u(L-\xi,t) = u(L+\xi,t) \quad \forall \xi \in [0,\delta] \tag{15}$$

Eq. (15) is the nonlocal homogeneous Neumann boundary condition, which admits a symmetric relation about boundary between real and fictitious domain. Let us note that a concentrate force at free boundary can be absorbed in body force associated with Dirac function.

3 Analytical solutions

3.1 Peristatic equation

Recall the one-dimensional peristatic equation obtained above

$$e\lambda(\delta) \int_{-\delta}^{\delta} \kappa(\xi) \left[u(x+\xi) - u(x)\right] d\xi + f(x) = 0 \tag{16}$$

Consider a rod fixed at both ends, as explained earlier. In this case the boundary conditions for non-local governing equation should be considered as

$$u(-\xi) = -u(\xi) \quad \text{and} \quad u(L-\xi) = -u(L+\xi) \quad \forall \xi \in [0,\delta] \tag{17}$$

Periodically extending Eq. (17) over the entire real line indicates that $u(x)$ is odd with respect to $x = nL$, $n = 0, 1, 2, \ldots$, as shown in Fig. 2. According to the periodicity property, $u(x)$ can be expressed in terms of the Fourier series as

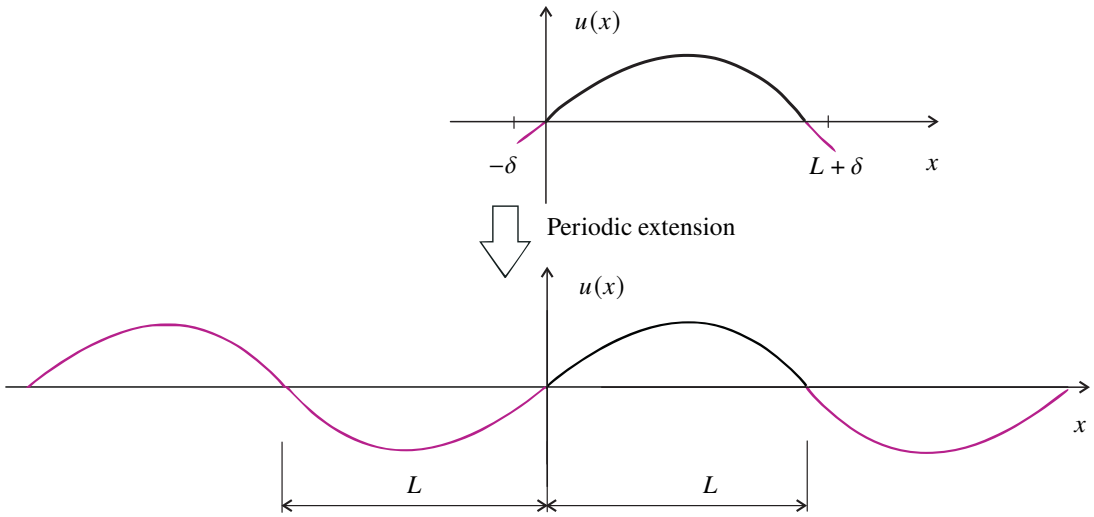

Fig. 2: Periodic extension of the displacement for fixed-fixed rod

$$u\left(x\right)=\sum_{n=1}^{\infty}b_n\sin\frac{n\pi x}{L} \tag{18}$$

Substituting Eq. (18) into (16) yields

$$\sum_{n=1}^{\infty}b_n\sin\frac{n\pi x}{L}\int_{-\delta}^{\delta}\kappa\left(\xi\right)\left(\cos\frac{n\pi\xi}{L}-1\right)d\xi=-\frac{f\left(x\right)}{e\lambda\left(\delta\right)} \tag{19}$$

where the coefficients can be obtained based on orthogonality

$$b_n=\frac{2}{Le\lambda\left(\delta\right)}\frac{\int_0^L f\left(x\right)\sin\frac{n\pi x}{L}dx}{\int_{-\delta}^{\delta}\kappa\left(\xi\right)\left(1-\cos\frac{n\pi\xi}{L}\right)d\xi} \tag{20}$$

Plugging Eq. (20) into (18) gives the complete solution to one-dimensional non-local Poisson's equation

$$u\left(x\right)=\frac{2}{Le\lambda\left(\delta\right)}\sum_{n=1}^{\infty}\frac{\int_0^L f\left(x\right)\sin\frac{n\pi x}{L}dx}{\int_{-\delta}^{\delta}\kappa\left(\xi\right)\left(1-\cos\frac{n\pi\xi}{L}\right)d\xi}\sin\frac{n\pi x}{L} \tag{21}$$

Regarding fixed-free BCs, as explained above the following conditions hold for non-local cases

$$u\left(-\xi\right)=-u\left(\xi\right),\quad\text{and}\quad u\left(L-\xi\right)=u\left(L+\xi\right)\quad\forall\xi\in\left[0,\delta\right] \tag{22}$$

If we periodically extend Eq. (22) over the entire real line, a function anti-symmetric with respect to $x=2nL$ and symmetric with respect to $x=\left(2n-1\right)L$ can be obtained as shown in Fig. 3. Based on such periodicity and symmetry, we can assume that the solution has the following form

$$u\left(x\right)=\sum_{n=1}^{\infty}b_n\sin\frac{\left(2n-1\right)\pi x}{2L} \tag{23}$$

Plugging Eq. (23) back into (16) gives

$$\sum_{n=1}^{\infty}b_n\sin\frac{\left(2n-1\right)\pi x}{2L}\int_{-\delta}^{\delta}\kappa\left(\xi\right)\left(\cos\frac{\left(2n-1\right)\pi\xi}{2L}-1\right)d\xi=-\frac{f\left(x\right)}{e\lambda\left(\delta\right)} \tag{24}$$

in which coefficients can be casted as

$$b_n=\frac{2}{Le\lambda\left(\delta\right)}\frac{\int_0^L f\left(x\right)\sin\frac{\left(2n-1\right)\pi x}{L}dx}{\int_{-\delta}^{\delta}\kappa\left(\xi\right)\left(1-\cos\frac{\left(2n-1\right)\pi\xi}{L}\right)d\xi} \tag{25}$$

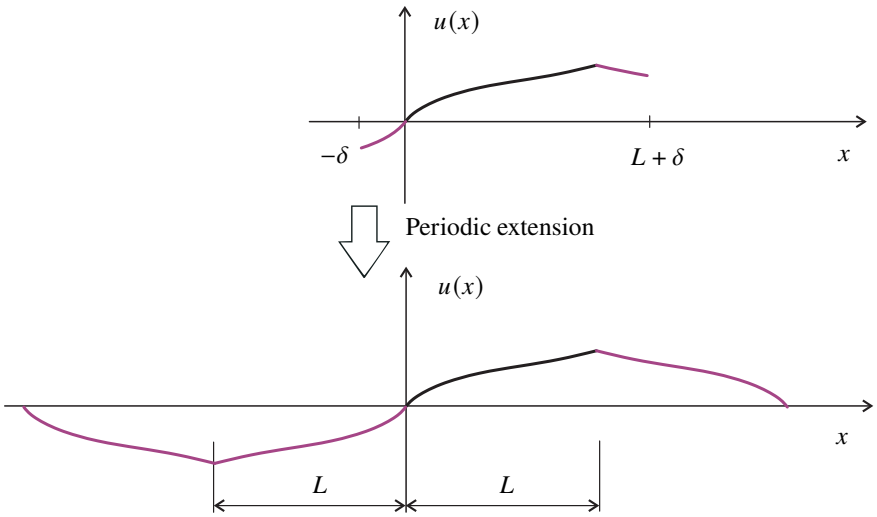

Fig. 3: Periodic extension of the displacement for fixed-free rod

Thus, by substituting Eq. (25) into (23), the complete solution for non-local Poisson's equation with fixed-free BCs can be given as

$$u(x) = \frac{2}{Le\lambda(\delta)} \sum_{n=1}^{\infty} \frac{\int_0^L f(x) \sin \frac{(2n-1)\pi x}{L} dx}{\int_{-\delta}^{\delta} \kappa(\xi) \left(1 - \cos \frac{(2n-1)\pi \xi}{L}\right) d\xi} \sin \frac{(2n-1)\pi x}{2L} \tag{26}$$

3.2 Peridynamic equation

Recall the non-local one-dimensional PD equation of motion

$$\ddot{u}(x,t) = \lambda(\delta) \int_{-\delta}^{\delta} \kappa(\xi) \left[u(x+\xi,t) - u(x,t)\right] d\xi \tag{27}$$

Let us separate spatial and time variables as follows

$$u(x,t) = X(x)\, T(t) \tag{28}$$

Plugging into Eq. (27) provides

$$X(x)\, \ddot{T}(t) = c\lambda(\delta) \int_{-\delta}^{\delta} \kappa(\xi) \left[X(x)\, T(t) - X(x+\xi)\, T(t)\right] d\xi \tag{29}$$

and consequently

$$\frac{1}{c\lambda(\delta)} \frac{\ddot{T}(t)}{T(t)} = \frac{1}{X(x)} \int_{-\delta}^{\delta} \kappa(\xi) \left[X(x) - X(x+\xi)\right] d\xi = -k, \tag{30}$$

where k is a parameter independent of x and t. The following two eigen-functions can be obtained as follows

$$\begin{aligned} &\ddot{T}(t) + kc\lambda(\delta)\, T(t) = 0, \\ &\int_{-\delta}^{\delta} \kappa(\xi) \left[X(x) - X(x+\xi)\right] d\xi = -kX(x) \end{aligned} \tag{31}$$

Let us first consider a (fixed-fixed) rod subject to some arbitrary initial conditions. By comparing Eq. $(31)_2$ with (16), we can consider $X(x)$ as an analogue to $u(x)$ and $-kX(x)$ to $-\frac{f(x)}{c\lambda(\delta)}$. Therefore, associating with Eq. (18), one can obtain that

$$X(x) = \sum_{n=1}^{\infty} b_n \sin \frac{n\pi x}{L} \tag{32}$$

and

$$\sum_{n=1}^{\infty} b_n \sin\frac{n\pi x}{L} \int_{-\delta}^{\delta} \kappa(\xi)\left(\cos\frac{n\pi\xi}{L} - 1\right) d\xi = -\sum_{n=1}^{\infty} k_n b_n \sin\frac{n\pi x}{L} \tag{33}$$

Thus, the eigenvalue can be casted as

$$k_n = \int_{-\delta}^{\delta} \kappa(\xi)\left(1 - \cos\frac{n\pi\xi}{L}\right) d\xi \tag{34}$$

By utilizing above result, the general solution to Eq. $(31)_1$ can be written as

$$T_n(t) = A_n^* \cos\left(\sqrt{k_n c\lambda(\delta)}t\right) + B_n^* \sin\left(\sqrt{k_n c\lambda(\delta)}t\right) \tag{35}$$

Coupling Eq. (32), (35) with (28), the general solution to Eq. (27) with fixed-fixed BCs can be formulated as

$$u(x,t) = \sum_{n=1}^{\infty}\left[A_n \cos\left(\sqrt{k_n c\lambda(\delta)}t\right) + B_n \sin\left(\sqrt{k_n c\lambda(\delta)}t\right)\right] \sin\frac{n\pi x}{L} \tag{36}$$

where the undetermined coefficients A_n and B_n depend on the initial conditions. Suppose that the following initial conditions are specified

$$u(x,0) = u_0(x), \quad \text{and} \quad \dot{u}(x,0) = v_0(x) \tag{37}$$

By associating with Eq. (36), one can obtain the following coefficients

$$A_n = \frac{2}{L}\int_0^L u_0(x) \sin\frac{n\pi x}{L} dx \quad \text{and} \quad B_n = \frac{2}{L}\frac{1}{\sqrt{k_n c\lambda(\delta)}}\int_0^L v_0(x) \sin\frac{n\pi x}{L} dx \tag{38}$$

By collecting the derivations above, the solution to one-dimensional non-local wave equation subjected to fixed-fixed boundary condition can be summarized as

$$u(x,t) = \sum_{n=1}^{\infty}\left[A_n \cos\left(\sqrt{k_n c\lambda(\delta)}t\right) + B_n \sin\left(\sqrt{k_n c\lambda(\delta)}t\right)\right] \sin\frac{n\pi x}{L} \tag{39}$$

with

$$\begin{aligned} A_n &= \frac{2}{L}\int_0^L u_0(x) \sin\frac{n\pi x}{L} dx, \quad B_n = \frac{2}{L}\frac{1}{\sqrt{k_n c\lambda(\delta)}}\int_0^L v_0(x) \sin\frac{n\pi x}{L} dx, \\ k_n &= \int_{-\delta}^{\delta} \kappa(\xi)\left(1 - \cos\frac{n\pi\xi}{L}\right) d\xi, \quad \lambda(\delta) = 2\left[\int_{-\delta}^{\delta} \kappa(\xi)\xi^2 d\xi\right]^{-1} \end{aligned} \tag{40}$$

In a similar manner, the solution to one-dimensional non-local wave equation subjected to fixed-free boundary condition can be given as follows

$$u(x,t) = \sum_{n=1}^{\infty}\left[A_n \cos\left(\sqrt{k_n c\lambda(\delta)}t\right) + B_n \sin\left(\sqrt{k_n c\lambda(\delta)}t\right)\right] \sin\frac{(2n-1)\pi x}{2L} \tag{41}$$

with

$$\begin{aligned} A_n &= \frac{2}{L}\int_0^L u_0(x) \sin\frac{(2n-1)\pi x}{2L} dx, \quad B_n = \frac{2}{L}\frac{1}{\sqrt{k_n c\lambda(\delta)}}\int_0^L v_0(x) \sin\frac{(2n-1)\pi x}{2L} dx \\ k_n &= \int_{-\delta}^{\delta} \kappa(\xi)\left[1 - \cos\frac{(2n-1)\pi\xi}{2L}\right] d\xi, \quad \lambda(\delta) = 2\left[\int_{-\delta}^{\delta} \kappa(\xi)\xi^2 d\xi\right]^{-1} \end{aligned} \tag{42}$$

4 Numerical examples

In order to analyze the influence of the kernel, several cases are tested and compared against the corresponding classical solutions. The following four kernel functions are taken into consideration

$$\begin{aligned}
\kappa_1(\xi) &= H(\xi+\delta) - H(\xi-\delta), \\
\kappa_2(\xi) &= \left(1 - \operatorname{sign}(\xi)\frac{\xi}{\delta}\right)[H(\xi+\delta) - H(\xi-\delta)], \\
\kappa_3(\xi) &= \frac{1}{|\xi|}[H(\xi+\delta) - H(\xi-\delta)], \\
\kappa_4(\xi) &= \exp\left[-\left(\frac{2\xi}{\delta}\right)^2\right][H(\xi+\delta) - H(\xi-\delta)],
\end{aligned} \tag{43}$$

where H denotes the Heaviside function. Figure 4 illustrates the kernel functions defined by Eqs (43).

4.1 Peristatic equation

Consider a rod subjected to a distributed load $f(x) = -f_a \sin(\pi x)$, where f_a is the loading amplitude. Figure 5 illustrates the normalized axial displacement as a function of the normalized axial coordinate. Four values of the horizon size are considered. To analyze the influence of the kernel function the plots of the displacements around the midpoint of the rod are enlarged. One can recognize that for the horizon size $\delta = 10^{-3}L$ the results of the non-local theory with different kernels almost coincide and correspond to the classical theory of rods. With an increase of the horizon size the increasing difference between the results is observed. The solution with the kernel function κ_4 provides the result which is closest to the classical one.
In the second case of fixed-free boundary conditions, the same model is chosen except right end is set free. Figure 6 shows the normalized axial displacement vs normalized axial coordinate. Similarly to the previous example, with an increase of the horizon size the difference between the classical solution and the solutions based on the non-local theory increases.

4.2 Free vibration

Consider the following initial conditions

$$u(x,0) = u_a \frac{x}{L}\left(\frac{x}{L} - 1\right)^2, \quad \dot{u}(x,0) = v_a \sin\left(\frac{\pi x}{L}\right), \quad v_a = 10^3 \frac{\sqrt{c}}{L} u_a,$$

where u_a and v_a are amplitudes of the displacement and velocity, respectively. Figure 7 shows the plots of the derived analytical solutions for the normalized axial displacement of the fixed-fixed rod as a function of the normalized time for different kernel functions and the horizon sizes. The same tendency as in the static cases is observed. The kernel function κ_4 leads to the smallest deviation to the classical solution for all selected horizon sizes.

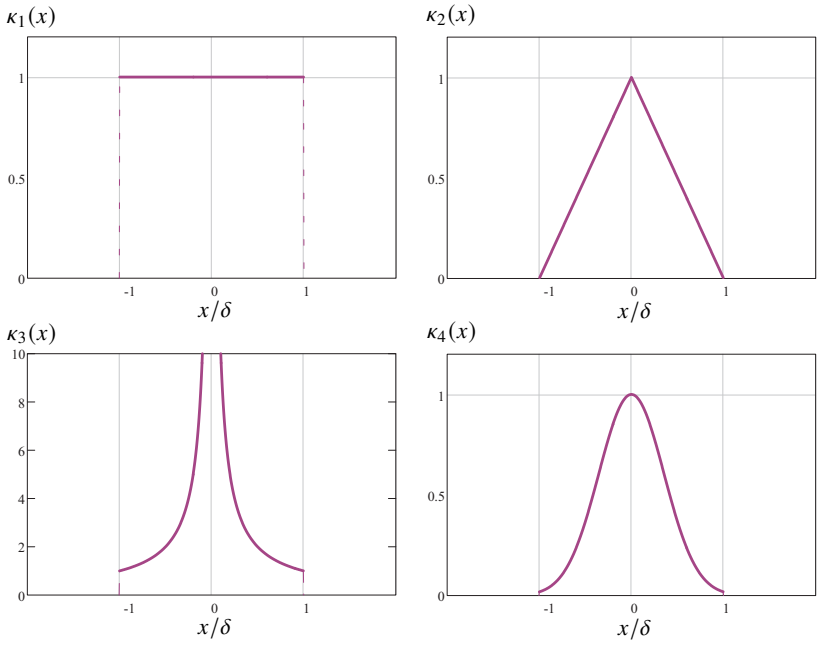

Fig. 4: Kernel functions defined by Eqs. (43)

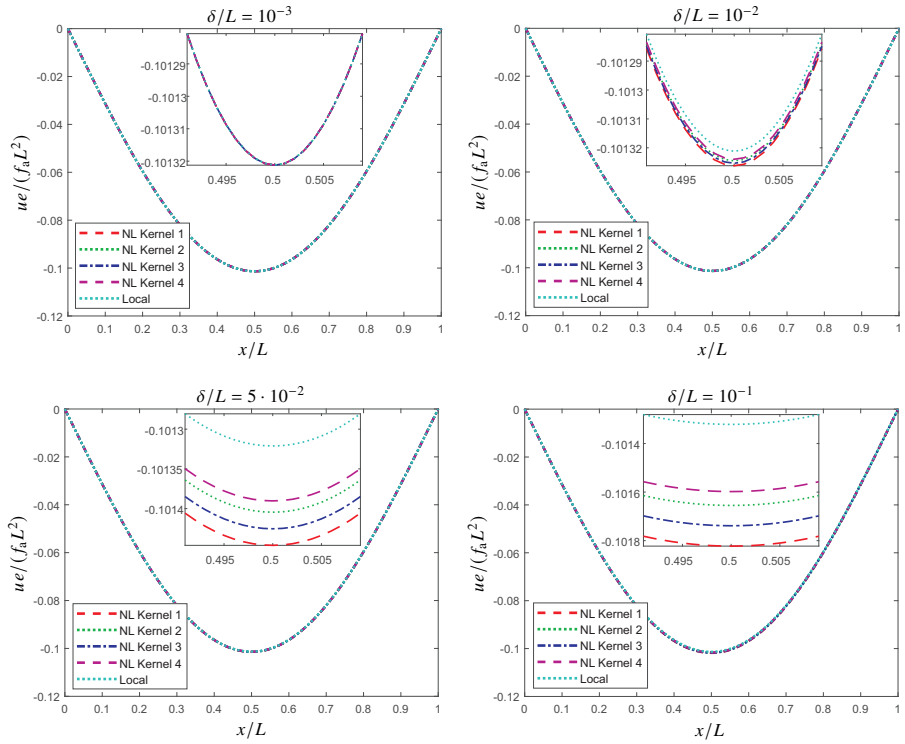

Fig. 5: Axial displacement in a statically loaded rod with fixed-fixed boundary conditions for different kernels and horizon sizes

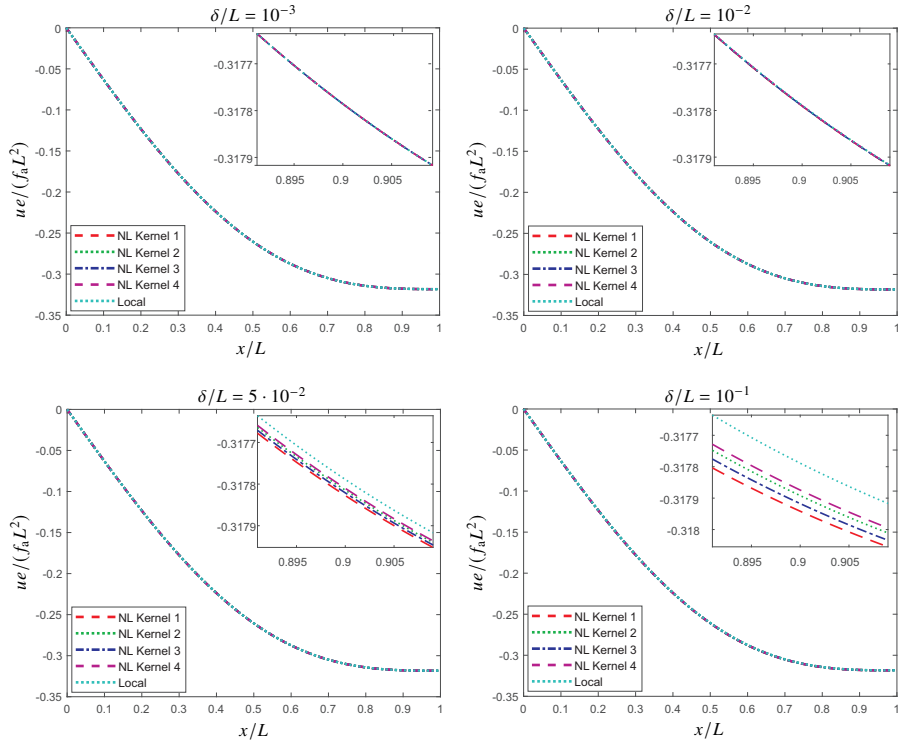

Fig. 6: Axial displacement in a statically loaded rod with fixed-fixed boundary conditions for different kernels and horizon sizes

Let us assume the following initial conditions

$$u\,(x,0) = u_{\mathrm{a}}\left[\left(\frac{x}{L}\right)^3 + \left(\frac{x}{L}\right)^2 + \frac{x}{L}\right], \quad \dot{u}\,(x,0) = v_{\mathrm{a}} \sin\left(\frac{\pi x}{L}\right), \quad v_{\mathrm{a}} = 10^3 \frac{\sqrt{c}}{L} u_{\mathrm{a}}$$

Figure 8 shows the normalized axial displacement as a function of the normalized time for the fixed-free boundary conditions. Compared to the previous case of fixed-fixed boundary conditions the results are more sensitive to the horizon size and to the type of the kernel function. Nevertheless similar tendency as in the previous case can be observed.

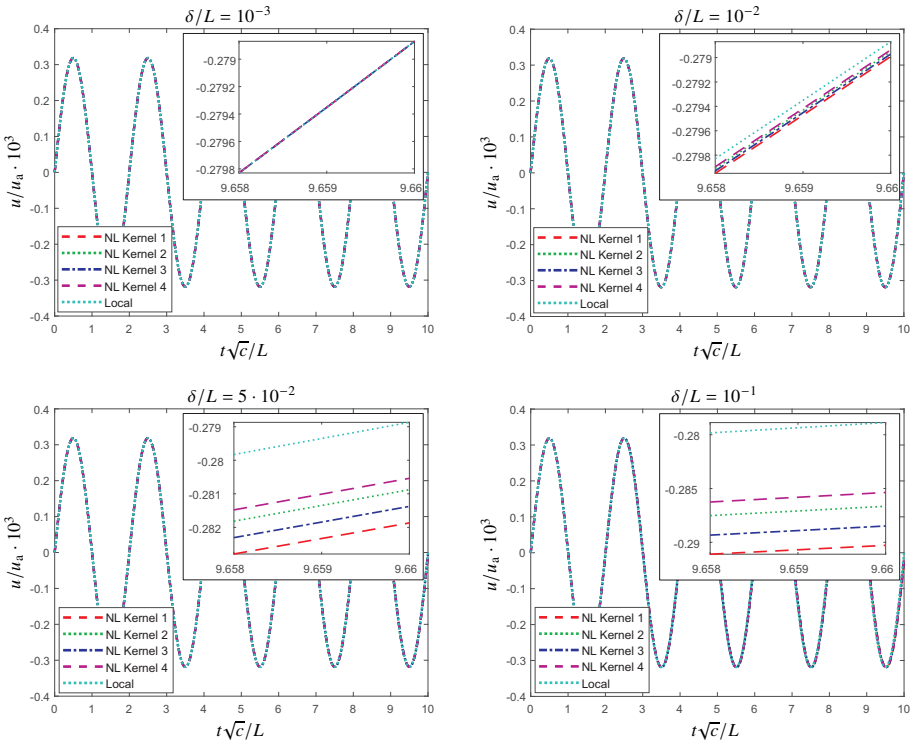

Fig. 7: Axial displacement in the point $x = L/2$ of a rod with fixed-fixed boundary conditions vs time for different kernels and horizon sizes

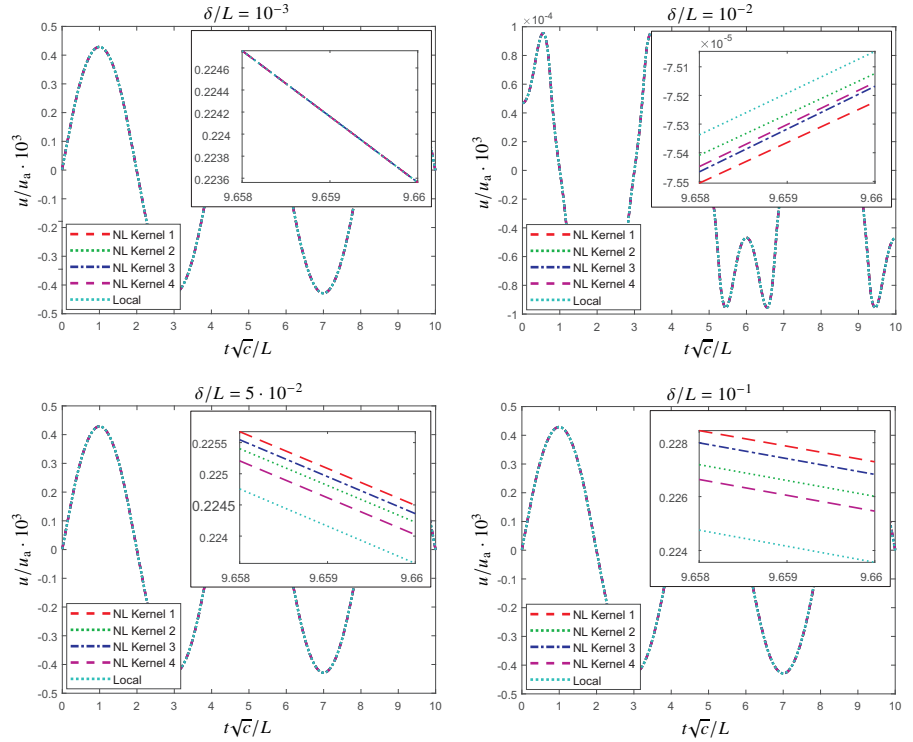

Fig. 8: Axial displacement in the point $x = 3L/4$ of a rod with fixed-free boundary conditions vs time for different kernels and horizon sizes

4.3 Frequencies

As illustrated above, kernels indeed play different roles in both statics and dynamics. In general PD converges to classical theory for small horizon size δ for all kernel cases, and diverge with increment of delta. In particular, the Gauss type kernel κ_4 provides the best approximation to the classical solution, followed by κ_2, κ_3 and κ_1.

In order to further investigate this subtlety, we compare the natural frequencies of PD and classical solution with gradual increment of horizon size delta. Figures 9 and Fig. 10, show the natural frequencies of first 6 modes of fixed-fixed rod and fixed-free rod,

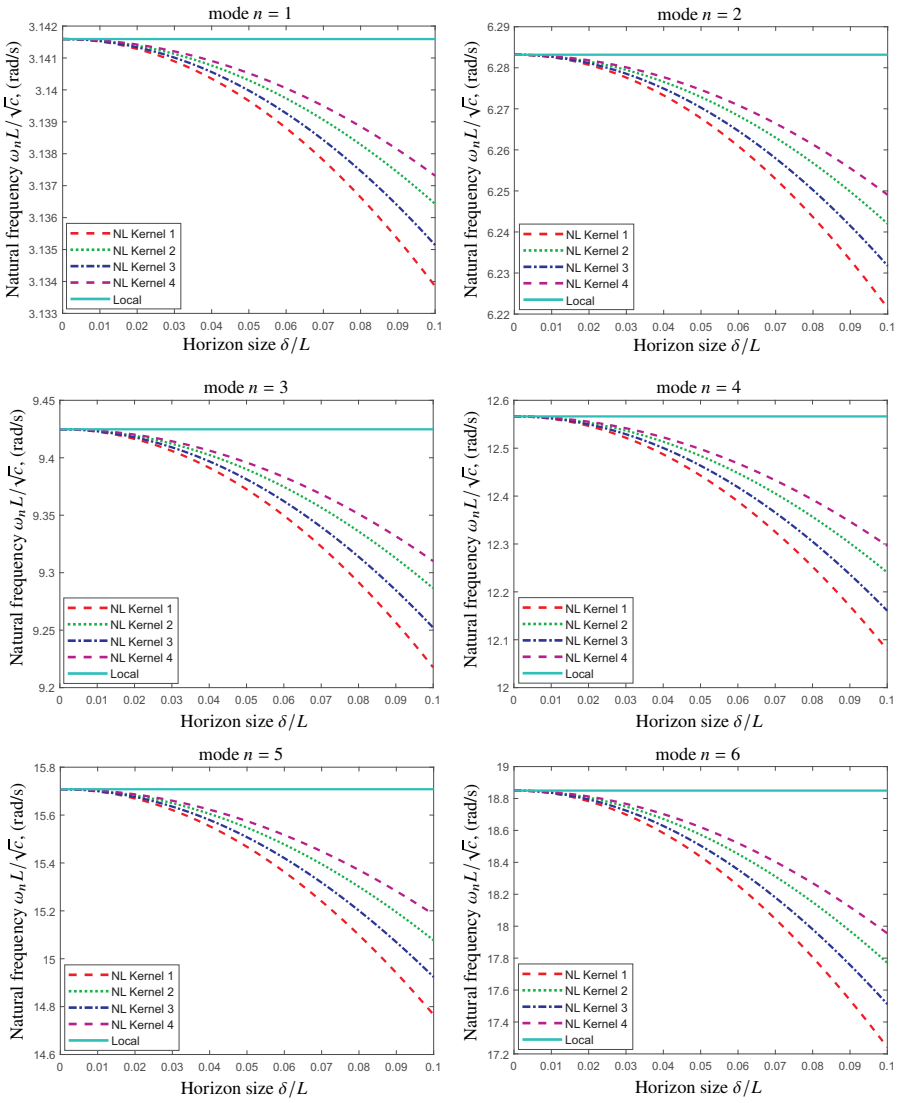

Fig. 9: Natural frequencies vs horizon size

respectively. Based on the results a similar conclusion can be made that PD solution converges to classical one as horizon delta approaches zero and diverges as delta increases.

5 Conclusions

This study provides a generalized PD formulation for one-dimensional rod structure and its analytical solutions. Based on the assumption of relations of PD pairwise interactions, various kernel functions can be selected. In particular, four common integration kernels are analyzed via benchmark problems. To validate the capacity, nonlocal results are compared against the corresponding classical solutions with consideration of different boundary conditions. One can observe that when the horizon size δ approaches zeros, the results according to the nonlocal theory converge to the classical results, while as δ increases, divergence emerges. This is reasonable, since as δ decreases, nonlocality of PD fades away and PD reduces to local theory consequently.
On the other hand, the introduced kernels play different roles in both statics and dynamics. In particular, the Gauss type kernel κ_4 gives the result which is closest to classical solution followed by κ_2, κ_3 and κ_1. For small values of the horizon size $\delta/L < 10^{-2}$ the difference between the solutions with different kernel functions becomes negligible.
The approach provided in this study can be extended to the analysis of two-dimensional structures, such as membranes, plates and shells. Furthermore,other physical problems such as heat diffusion and acoustics can be analyzed within the framework of PD.

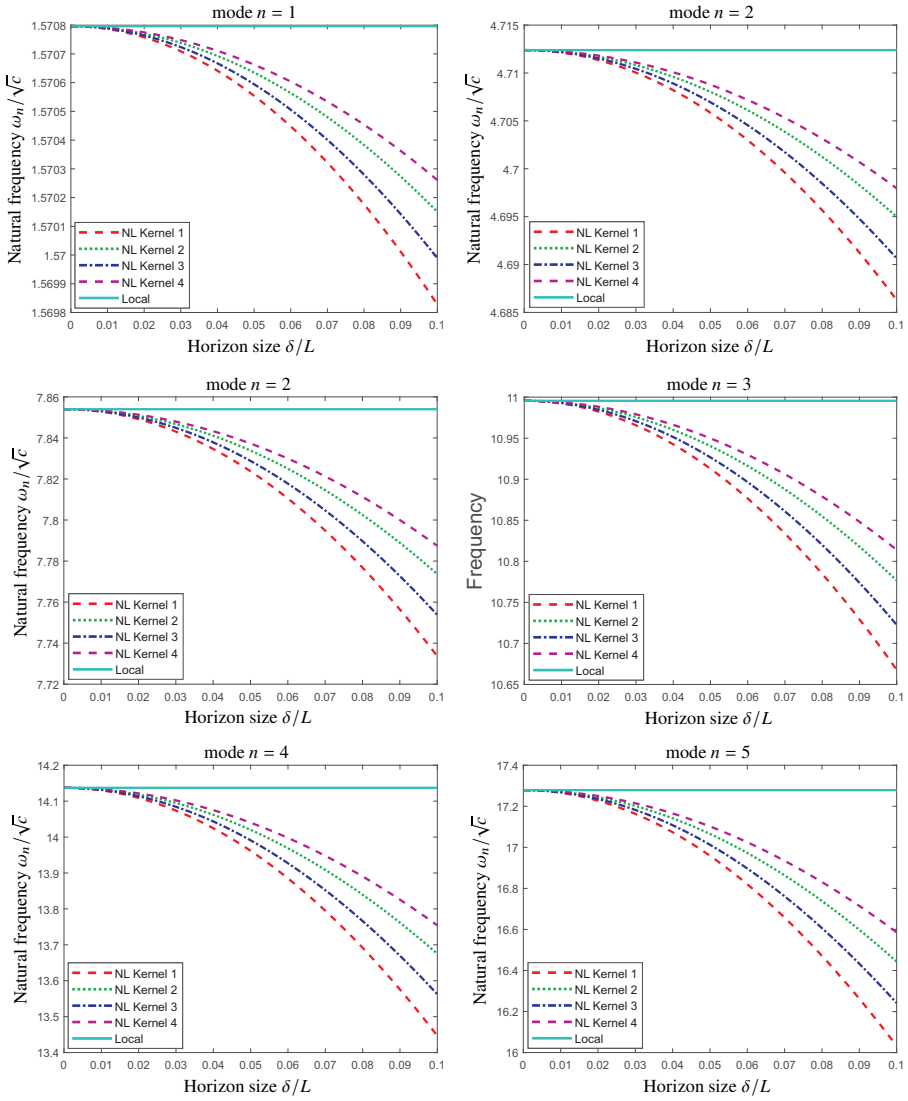

Fig. 10: Natural frequencies vs horizon size

References

Shubhankar Roy Chowdhury, Pranesh Roy, Debasish Roy, and JN Reddy. A peridynamic theory for linear elastic shells. *International Journal of Solids and Structures*, 84:110–132, 2016. doi: https://doi.org/10.1016/j.ijsolstr.2016.01.019.

Nicolas M Cordero, Samuel Forest, and Esteban P Busso. Second strain gradient elasticity of nano-objects. *Journal of the Mechanics and Physics of Solids*, 97:92–124, 2016. doi: https://doi.org/10.1016/j.jmps.2015.07.012.

Vito Diana and Roberto Ballarini. Crack kinking in isotropic and orthotropic micropolar peridynamic solids. *International Journal of Solids and Structures*, 196:76–98, 2020. doi: https://doi.org/10.1016/j.ijsolstr.2020.03.025.

Victor A Eremeyev. Strong ellipticity and infinitesimal stability within n th-order gradient elasticity. *Mathematics*, 11(4):1024, 2023. doi: https://doi.org/10.3390/math11041024.

Javad Mehrmashhadi, Mohammadreza Bahadori, and Florin Bobaru. On validating peridynamic models and a phase-field model for dynamic brittle fracture in glass. *Engineering Fracture Mechanics*, 240:107355, 2020. doi: https://doi.org/10.1016/j.engfracmech.2020.107355.

Yozo Mikata. Analytical solutions of peristatic and peridynamic problems for a 1D infinite rod. *International Journal of Solids and Structures*, 49(21):2887–2897, 2012. doi: https://doi.org/10.1016/j.ijsolstr.2012.02.012.

Yozo Mikata. Analytical solutions of peristatics and peridynamics for 3d isotropic materials. *European Journal of Mechanics-A/Solids*, page 104978, 2023. doi: https://doi.org/10.1016/j.euromechsol.2023.104978.

Konstantin Naumenko and Victor A. Eremeyev. A non-linear direct peridynamics plate theory. *Composite Structures*, 279:114728, 2022. doi: https://doi.org/10.1016/j.compstruct.2021.114728.

Konstantin Naumenko, Matthias Pander, and Mathias Würkner. Damage patterns in float glass plates: Experiments and peridynamics analysis. *Theoretical and Applied Fracture Mechanics*, 118:103264, 2022. doi: https://doi.org/10.1016/j.tafmec.2022.103264.

Vinesh V Nishawala and Martin Ostoja-Starzewski. Peristatic solutions for finite one-and two-dimensional systems. *Mathematics and Mechanics of Solids*, 22(8):1639–1653, 2017. doi: https://doi.org/10.1177/1081286516641180.

Bo Ren, CT Wu, and E Askari. A 3D discontinuous Galerkin finite element method with the bond-based peridynamics model for dynamic brittle failure analysis. *International Journal of Impact Engineering*, 99:14–25, 2017. doi: https://doi.org/10.1016/j.ijimpeng.2016.09.003.

Stewart A Silling. Introduction to peridynamics. In *Handbook of peridynamic modeling*, pages 63–98. Chapman and Hall/CRC, 2016.

Stewart A Silling and Ebrahim Askari. A meshfree method based on the peridynamic model of solid mechanics. *Computers & structures*, 83(17-18):1526–1535, 2005. doi: https://doi.org/10.1016/j.compstruc.2004.11.026.

Stewart A Silling and Richard B Lehoucq. Peridynamic theory of solid mechanics. *Advances in applied mechanics*, 44:73–168, 2010. doi: https://doi.org/10.1016/S0065-2156(10)44002-8.

Stewart A Silling, Markus Zimmermann, and Rohan Abeyaratne. Deformation of a peridynamic bar. *Journal of Elasticity*, 73(1): 173–190, 2003. doi: https://doi.org/10.1023/B:ELAS.0000029931.03844.4f.

William Weaver Jr., Stephen P Timoshenko, and Donovan Harold Young. *Vibration problems in engineering*. John Wiley & Sons, 1991.

Olaf Weckner and Rohan Abeyaratne. The effect of long-range forces on the dynamics of a bar. *Journal of the Mechanics and Physics of Solids*, 53(3):705–728, 2005. doi: https://doi.org/10.1016/j.jmps.2004.08.006.

Zhenghao Yang, Chien-Ching Ma, Erkan Oterkus, Selda Oterkus, and Konstantin Naumenko. Analytical solution of 1-dimensional peridynamic equation of motion. *Journal of Peridynamics and Nonlocal Modeling*, pages 1–19, 2022a. doi: https://doi.org/10.1007/s42102-022-00086-1.

Zhenghao Yang, Konstantin Naumenko, Holm Altenbach, Chien-Ching Ma, Erkan Oterkus, and Selda Oterkus. Some analytical solutions to peridynamic beam equations. *ZAMM-Journal of Applied Mathematics and Mechanics/Zeitschrift für Angewandte Mathematik und Mechanik*, 102(10):e202200132, 2022b. doi: https://doi.org/10.1002/zamm.202200132.

Zhenghao Yang, Konstantin Naumenko, Chien-Ching Ma, Holm Altenbach, Erkan Oterkus, and Selda Oterkus. Some closed form series solutions to peridynamic plate equations. *Mechanics Research Communications*, 126:104000, 2022c. doi: https://doi.org/10.1016/j.mechrescom.2022.104000.